Micromachines **2015**, *6*, 879-901; doi:10.3390/mi6070879

OPEN ACCESS

micromachines

ISSN 2072-666X

www.mdpi.com/journal/micromachines

Review

Micromachined Shape-Memory-Alloy Microactuators and Their Application in Biomedical Devices

Mohammad Amri Zainal [1], Shafishuhaza Sahlan [1] and Mohamed Sultan Mohamed Ali [1,2,*]

[1] Faculty of Electrical Engineering, Universiti Teknologi Malaysia, 81310 Skudai, Johor, Malaysia; E-Mails: mamri3@live.utm.my (M.A.Z.); shafis@fke.utm.my (S.S.)

[2] Flextronics, Pelabuhan Tanjung Pelepas (PTP), 81560 Gelang Patah, Johor, Malaysia

* Author to whom correspondence should be addressed; E-Mail: sultan_ali@fke.utm.my; Tel.: +60-7-5557165; Fax: +60-7-5566272.

Academic Editor: Miko Elwenspoek

Received: 16 March 2015 / Accepted: 19 May 2015 / Published: 10 July 2015

Abstract: Shape memory alloys (SMAs) are a class of smart materials characterized by shape memory effect and pseudo-elastic behavior. They have the capability to retain their original form when subjected to certain stimuli, such as heat or a magnetic field. These unique properties have attracted many researchers to seek their application in various fields including transportation, aerospace, and biomedical. The ease process adaption from semiconductor manufacturing technology provides many opportunities for designing micro-scale devices using this material. This paper gives an overview of the fabrication and manufacturing technique of thin-film and bulk micromachined SMAs. Key features such as material properties, transformation temperature, material composition, and actuation method are also presented. The application and micromechanism for both thin-film and bulk SMA are described. Finally, the microactuator devices emphasized for biomedical applications such as microgrippers and micropumps are highlighted. The presented review will provide information for researchers who are actively working on the development of SMA-based microscale biomedical devices.

Keywords: thin-film shape memory alloy; bulk shape memory alloy; microactuator; micropump; biomedical

---

1. Intro duction

Today, there is significant attention from the research community for a class of materials called stimulus-responsive materials (SRMs), which are able to respond to a certain stimulus, such as, chemical, light or heat. According to Sun *et al.* [1], in their extensive review paper on SRMs, this class of materials can be divided into two groups, shape change material (SCM) and shape memory materials (SMMs). Among the types of SMMs that have been developed so far are shape memory polymers (SMPs), shape memory hybrid (SMH), and shape memory alloy (SMA) [2].

Over the years, SMA has been used in diverse applications, such as in transportation [3], aerospace [4,5], and biomedical fields [6]. One of the advantages of SMA compared to the other types of SMMs is the high actuation stress it can provide. Others attractive features of SMA include its ability to provide large strain during mechanical loading (also known as pseudoelasticity), shape recovery upon heating (shape memory effect, SME), and biocompatibility, which make SMA one of the preferred actuators, particularly in biomedical applications. Micromachined SMA microactuators, for example, have been investigated in an extensive range of biomedical areas, including endovascular surgery [7], intestinal obstruction [8], neural interfaces [9], and drug delivery [10]. For these types of applications, a nickel titanium (NiTi) SMA composition is commonly used. Although it is known that pure Ni is a toxic element, Ni-hypersensitivity of the human body has not been reported [11]. While research on Ni-free Ti-based SMAs for biomedical applications is still ongoing [12–15], NiTi is still among the popular SMAs in biomedical applications.

Despite their favorable features, SMA microactuators possess several drawbacks. One of the limiting factors is SMA formation with a desired transformation temperature. In general, there are two commonly used approaches in fabricating SMA microactuators. In the first technique, a thin-film of SMA is deposited on a substrate. Since the alloy composition, which affects the transformation temperature, can be varied, this technique is preferred. However, the transformation temperature is very sensitive to metallurgical factors such as aging and annealing treatment [16]. In addition, the limited film thickness restricts the mechanical performance of the SMA. Nonetheless, this drawback can be overcome by using bulk SMAs, which are commercially available in a range of thicknesses. Thus far, successful applications of bulk-micromachined SMA microactuators have been demonstrated in various works in the literature [17–19]. Besides its mechanical robustness, the bulk-micromachined SMA is also cost effective as expensive equipment is not required for the fabrication and crystallization of this material. In spite of these advantages, to alter the transformation temperature, additional processes such as constraint annealing must be carried out [20]. In addition to that, fabrication that involves bulk materials is not compatible with standard microfabrication processes and could result in additional costs and complex fabrication procedures.

In this paper, a review of the use of thin-film and bulk NiTi SMA in microactuators with an emphasis on the material properties, fabrication techniques, and actuation methods is presented. Detailed information on the SMA transformation temperatures and material composition is given based on the review carried out. The fabrication of thin-film and bulk SMA is also thoroughly discussed along with relevant literature. Finally, devices and other biomedical devices are reviewed and reported.

2. Thin-Film SMA

A thin-film is a layer that is normally formed by the vapor-deposition process. It can be fabricated by deposition of individual atoms on a substrate. The study of thin-film material started back in the nineteenth century. While research on SMA began in the early 1930s [1], initial attempts at integrating NiTi thin-film SMA in microelectromechanical systems (MEMS) only started in 1990, when it was demonstrated by Walker *et al.* [21].

The most common method for depositing NiTi thin-film is sputter deposition. Among the well-known types of sputtering system are DC magnetron [22–24], Radio Frequency (RF) magnetron [25,26], and ion-beam systems [27]. Besides sputtering, other reported methods include flash evaporation [28,29], pulsed laser deposition [30–34], filtered arc deposition [35], cluster beam deposition [36], and cathodic arc plasma ion plating [37]. By using the sputtering technique, a film with a thickness of up to 30 μm can be deposited, as reported in [38]. In sputter deposition, atoms are ejected from the target sourceand deposited onto a substrate due to bombardment of high-energy particles from sputtering gas such as argon. This technique allows the deposition to be performed at low temperature [39], thus eliminating thermal coefficient mismatch with the substrate and the deposited thin-film. Moreover, the deposition process can be tailored to achieve the desired transformation temperature by varying either the target material composition or the *in-situ* deposition parameters [40,41]. This technique, however, poses a challenge in term of controlling the thin-film composition resulting from differences in sputtering yields from the target material. Parameters used during sputtering such as air purity during the vacuum process, gas pressure, temperature, annealing, sputtering power, and so on must be optimized to get the desired stoichiometry, which has an effect on the properties and characteristics of the thin-film.

Apart from the uniformity issue [42], sputter-deposited NiTi thin film is known to have a slight deficiency in the Ti element compared with the target alloy [43]. To overcome this problem, the co-sputtering technique has been investigated using either separate targets for Ni and Ti [44] or NiTi with an additional Ti target [41,45,46]. In [41], Schell *et al.* reported the possibility of using *in-situ* X-ray diffraction (XRD) to design the phase content of NiTi SMA thin-films by varying the power of co-sputtering NiTi with an additional Ti target. Although the thin-films are successfully controlled and manipulated in real-time, this setup requires additional equipment such as XRD and X-ray reflectivity (XRR) to be integrated into the available sputtering system. This will significantly increase the cost and complexity of the overall system. A less complex, and more economical method, of depositing Ti-rich NiTi SMA was reported by Seong *et al.* [44]. In [44], co-sputtered thin-films were sandwiched between two Ti plates prior to heat treatment to make them Ti-rich. This technique eliminates extra equipment and procedures compared with the technique performed by [41].

A small change (a fraction of one percent) in alloy composition can cause significant differences in the shape memory properties and transformation temperature [47,48]. The effect of different atomic compositions of NiTi thin-films on the transformation temperature is shown in Table 1. This table is a data compilation of NiTi thin-films fabricated by several researchers with characteristic temperatures associated with phase change: martensite finish (M_f), martensite start (M_s), austenite start (A_s), and austenite finish (A_f). At room temperature, all compositions were in the martensite phase except for the compositions reported in [35,49]. This is in accordance with the fact that Ti-rich thin-film has a transformation temperature near to or above ambient temperature. The film composition is not the only

factor that affects the transformation temperature. Surbled *et al.* [16] reported that Ti-rich film also showed a strong dependence of transformation temperature on heat treatment. The transformation temperature and the transformation temperature hysteresis decrease with the decrease of annealing temperature. This was shown by the compositions in [44,50], which have the same atomic percentage but different annealing parameters. The temperature range for the composition in [44] increased slightly to around 13–27 °C, compared to the composition in [50]. The same is true for the compositions in [51,52].

Table 1. Different compositions of NiTi thin-film shape memory alloys (SMAs) fabricated by several researchers.

References	Deposition Type	Atomic Composition	M_f (°C)	M_s (°C)	A_s (°C)	A_f (°C)	Annealing Temperature (°C)	Annealing Duration (h)
Yang *et al.* [35]	Filtered arc	$Ni_{51.0at\%}Ti_{49.0}$	−9	49	4	71	not available	not available
Kim *et al.* [44]	Co-sputtering	$Ni_{49.4at\%}Ti_{50.6}$	57	63	86	100	700	10
Chun *et al.* [49]	Sputtering	$Ni_{49.5at\%}Ti_{50.5}$	−17	−3	22	35	500	2
Sanjabi *et al.* [50]	Co-sputtering	$Ni_{49.4at\%}Ti_{50.6}$	30	50	71	86	500	1
Liu *et al.* [51]	Sputtering	$Ni_{47.4at\%}Ti_{52.6}$	55	70	80	95	600	not available
Mohanchandra *et al.* [52]	Sputtering	$Ni_{47.5at\%}Ti_{52.5}$	45	66	81	98	500	2

Besides the transformation temperature, another important feature of SMA is the SME, which can be described as the ability of the material to recover its original shape. The phase transition from martensite to austenite occurs when the alloy is heated and the material temperature has reached A_f. In this phase, the alloy will regain its deformed shape. Cooling the alloy until it reaches M_f will not cause any physical change. This behavior is called the one-way shape memory effect (OWSME). The two-way shape memory effect (TWSME), however, can exhibit a repeatable shape change under no applied load and thus minimizes the complexity of the actuator's construction. In other words, the alloy can remember its shape in both martensite and austenite phases. Freestanding films usually show intrinsic TWSME, with large displacement, but relatively small force in actuation [53]. Several studies and approaches have been carried out to fabricate TWSME thin-film SMA. Among these are approaches that employ gradation of composition across the film thickness. Ho *et al.* [43] reported a novel sputtering procedure to compensate Ti deficiency from a single near-equiatomic NiTi target. In [43], the target was gradually heated up to 700 °C to obtain compositional variation through the film thickness. The transformation temperature varies as result of this, which in turn builds different internal stresses throughout the film thickness. A similar procedure was reported in [54], where TWSME NiTi thin-film is successfully fabricated with a transformation temperature above 25 °C. In [54], NiTi thin-film was deposited on 1 mm-thick $Ni_{56at\%}Ti_{44}$ substrate by using $Ni_{47at\%}Ti_{53}$ as a target. Annealing of the films produced a compositional gradient throughout the film-substrate interface as a result of diffusion. This procedure eliminated the extra power needed to heat up the target as done by Ho *et al.* [43], and hence reduced the cost. Another method of obtaining composition gradation in thin-films is by co-sputtering using both NiTi and Ti targets and varying the target power [55,56]. Varying the target power affects the sputtering rate of each target, resulting in gradation of the thin-film.

The other factor that contributes to TWSME is the precipitation process. The precipitate formation is normally obtained by aging and is very sensitive to heat treatment. For this reason, Sato *et al.* [57] studied the optimum aging conditions for TWSME of sputter-deposited thin film. They reported that

sputter-deposited Ni-rich $Ni_{51.3at\%}Ti_{48.7}$ thin-film showed excellent TWSME when aged under constraints at 400 °C for 100 h. They observed that the film aged at 300 °C showed different behavior from the film aged at 500 °C, even with the same aging time, as shown in Figure 1. In boiling water, both films bent in the same direction as the constrained direction (Figure 1a,c), but in iced water, the film aged at 300 °C bent forward (Figure 1b), while the film aged at 500 °C bent backward and showed the opposite curvature (Figure 1d). One of the advantages of utilizing precipitation process to obtain TWSME of thin-film SMA is high strain compared to that of compositional gradation TWSME. However, the techniques mentioned above require high temperature for crystallization to enable the SME in NiTi SMA thin-films. Such a requirement is not a feasible option especially in MEMS fabrication process especially when material with low melting point is used. However, local annealing using laser beam might provide a solution to this problem [58,59]. With this technique, the annealed part of NiTi thin-films will exhibit SME while the non-annealed regions demonstrating elastic behavior [60] without affecting the integrity of the other parts of the device.

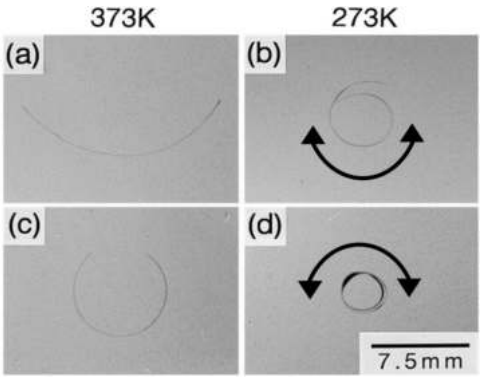

Figure 1. Spontaneous shape change of $Ti_{51.3at\%}Ni$ thin films aged at (**a**,**b**) 573 K for 1 h and (**c**,**d**) 723 K for 1 h: (**a**,**c**) in boiling water; and (**b**,**d**) in iced water. The thin films are seen from the side. Reprinted with permission from [57], copyright 1998 Elsevier.

3. Bulk Micromachined SMA

The methods of manufacturing bulk NiTi SMA can be classified into two categories: casting and powder metallurgy. The commercial casting process of NiTi SMA requires arc or induction melting of Ni and Ti elements. The widely use methods for this case are vacuum induction melting (VIM) and vacuum arc remelting (VAR). As the names suggest, both processes are done under vacuum. In VIM (Figure 2), the AC current is the source of the magnetic field produced by an induction coil. This electromagnetic induction is later used to induce electrical eddy currents in the metals and graphite crucible, which heat up and eventually melt the element. The advantage of this process is that the stirring of the melt is done naturally by electrodynamic force, thus yielding good microstructural and chemical homogeneity. The graphite crucible is used because of its excellent chemical homogeneity. However, it is known that NiTi melts dissolve carbon from the crucible during solidification and hence can alter the transformation behavior [61]. Several studies aiming to minimize this issue have been reported. These include the use of Ti-disk cladding [62], deploying a charging sequence and creating a screen of Titanium-Carbon on the inner surface of the graphite crucible [63], and replacing the graphite crucible with a water-cooled copper mold (copper boat) [64].

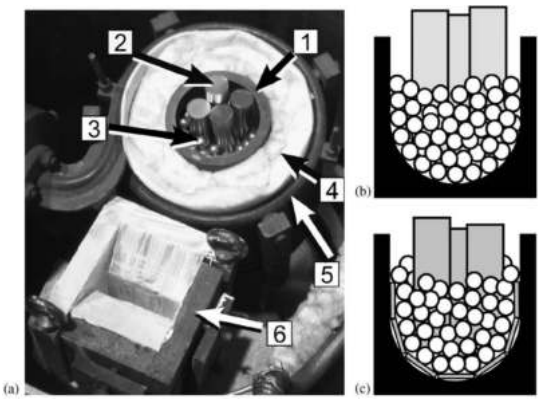

Figure 2. (**a**) Photograph of the graphite crucible with Ti rods and Ni pellets (1, graphite crucible; 2, Tirods; 3, Nipellets; 4, isolation; 5, water-cooled copper coil; and 6, mold); (**b**) schematic illustration of crucible filling: Ni pellets are in contact with the graphite crucible and Ti rods stick in the Ni pellets; and (**c**) the same as in (**b**), but a Ti-disk cladding prevents direct contact between Ni and graphite. Reprinted with permission from [62], copyright 2004 Elsevier.

Meanwhile, in the VAR method, a carbon graphite crucible is not required, thus eliminating the carbon contamination. Melting in VAR is done by an electrical arc discharge between a tungsten electrode and constituent elements, which is carried out in a water-cooled copper crucible. Unlike in VIM, there are no electromagnetic forces to naturally stir the molten material. Therefore, several remelting processes are required to obtain high purity yields and homogeneity. Proper attention to the number of melting cycles, ingot homogeneity, and oxygen pick-up can give a high-quality NiTi mold [65]. Several high remelting cycles for homogenization are reported in some works in the literature. In Lin *et al.* [66], homogenization is performed at 1050 °C for 72 h, while in Shamir *et al.* [67], hot forging and annealing are performed at 1000 °C for 12 h after several remelting cycles for homogenization. The high temperature and long duration of annealing can be considered as an important disadvantage of the VAR method.

An alternative to the VIM and VAR methods for fabricating bulk SMA is Electron Beam Melting (EBM). In this process, the carbon contamination is completely eliminated since the melting process is done in a water-cooled copper crucible. The oxygen contamination is minimized since the process takes place in a high vacuum. Otubo *et al.* [68] reported that EBM produced NiTi SMA and was a viable process resulting in ingots with a carbon content as low as 70 ppm. It also showed that the martensitic transformation is decreased by the presence of carbon and oxygen and depending upon the degree of contamination, where the deviation from the reference curve can be as high as 100 °C.

In terms of mechanical properties, bulk SMA offers some advantages over the thin-film counterpart. The TWSME in bulk SMA is always preferable due to its high actuation force. However, the TWSME is not an inherent property in bulk SMA but it is possible to acquire the effect intrinsically through training. There are several training methods reported in the literature, most of which are associated with thermomechanical processes. These include constraint annealing [20,69–74] and stress (tensile or compressive) loading cycles [75–80]. The thermomechanical training is known to be an effective way to acquire TWSME, but the amount and stability of this effect are difficult to control [20]. An example of constraint annealing is given in a work done by Wang *et al.* [20]. In [20], the SME behavior of a

NiTi-based SMA spring trained by constrained annealing treatment is investigated. $Ni_{50.8at\%}Ti_{49.2}$ wires were wound and fixed on a spiral cylinder shape (Figure 3). Then the fixture was annealed at 650 °C for 2 h, followed by water quenching. The spring was later elongated to a desired length with a similar fixture following annealing at 500 °C for 2 h and cooled naturally for one cycle. The shape memory strain from austenite to R-phase was greater than that from R-phase to martensite, which indicated a significant R-phase transformation in TWSME. Another configuration is seen in Costanza *et al.* [74], where wound and locked Ti-rich SMA wires on commercial screws with constant pitch are reported. In this configuration, the SMA was annealed at 500 °C for 15 min and quenched in water to impress the elongated shape into the SMA spring. Both thermomechanical processes mentioned above have to undergo a long annealing process to acquire TWSME. This processing time could, however, be reduced by applying a stress loading cycles to form the TWSME.

Apart from TWSME, there is also a report on realizing triple-way shape memory effect (TRSME) using bulk SMA. In TRSME, the material can recover from temporary shape to original shape through two intermediate predefined shapes. Unlike the SMPs that have much attention from researchers of the TRSME [81–84], the research progress of such effect in SMA is somehow stagnant. To the best knowledge of the authors, the only study of TRSME in SMA is reported by Tang *et al.* [85]. In [85], the results shows that the TRSME can be achieved only in those NiTi SMA with R-phase, provided that the temperature range between R-phase to austenite and martensite to austenite is over 10 °C.

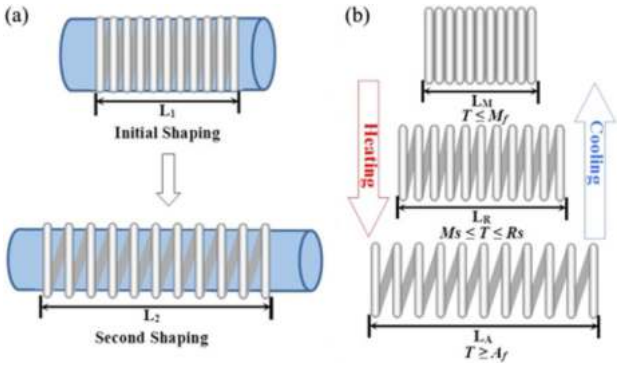

Figure 3. Diagrammatic representation of (**a**) constraint annealing in the whole manufacturing process and (**b**) springs with TWSME. Reprinted with permission from [20], copyright 2013 Springer.

4. Actuation Methods and Applications

4.1. Thin-Film SMA Actuator

The actuation scheme of SMA is selected based on specific applications. Generally, there are two types of actuation schemes that are commonly used: out-of-plane displacement and linear displacement. Among the devices using out-of-plane displacement scheme are micropumps, which utilize a thin-film to form a diaphragm type actuator as reported by Nisar *et al.* [86] and shown in Figure 4. From Figure 4, assuming that the diaphragm deformation is downward, the fluid is forced out to the outlet check valve when the pump chamber contracts, while the inlet check valve ensures that there is no back flow to the reservoir. Reciprocally, the fluid is forced into the inlet check valve when the pump chamber expands,

while the outlet check valve prevents back flow from the outlets. The two-way actuation can be obtained by polyimide-spring bias [87], two-way antagonistic actuation [87], an SMA-Si driving membrane [88], and gas pressurization [89,90]. Another actuator that utilizes thin-film SMA to provide out-of-plane displacement is the cantilever type actuator. Normally, one end of the cantilever will be fixed while the other end will provide displacement upon heating or cooling depending on the SMA properties. Among the latest studies of this kind of actuator is one reported by Wongweerayoot *et al.* [91]. In [91], a 5 μm thick NiTi thin film was deposited on a freestanding copper structure forming a bimorph microgripper. According to the report, the microgripper was able to grasp and hold a small plastic ball weighing around 0.5 mg (Figure 5). However, the cantilever type actuators produce a large stroke but yield a smaller force compared to diaphragm type actuators [38]. Nevertheless, this shortcoming can be compensated for using a bulk SMA cantilever type actuator.

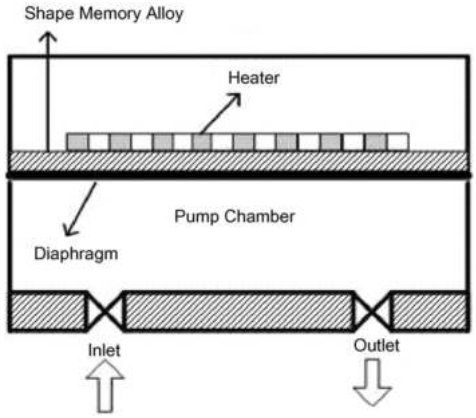

Figure 4. Schematic illustration of SMA micropump, as illustrated by Nisar *et al*. Reprinted with permission from [86], copyright 2008 Elsevier.

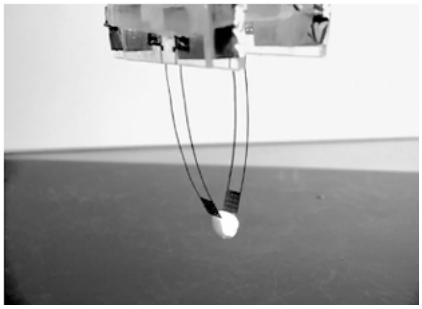

Figure 5. Captured image of microgripper grasping, lifting, and holding a small plastic ball. Reprinted with permission from [91], copyright 2014 Springer.

4.2. Bulk Micromachined-SMA Actuator

Various forms of bulk SMA are used to fabricate actuators. These include SMA wires, tubes, and sheets. It is common to fabricate cantilever type actuators by using an SMA sheet because of the high actuation force compared with thin-film SMA. The two-way actuation can be obtained through mechanical TWSME [1], such as depositing a reset layer (SiO_2 or Si_3N_4) on the SMA [92–94], as shown in Figure 6, or by using intrinsic TWSME [25]. The actuation is normally performed using Joule heating by passing the current through the SMA itself.

Figure 7 shows the deflection tip during the austenite to martensite phase of the cantilever-type actuator. The total displacement can be varied by controlling the deposition length of SiO_2/Si_3N_4 on the SMA. The deformation is attained as a result of the difference between the coefficients of thermal expansion (CTE) of the NiTi and SiO_2 that form the bimorph. At room temperature, the SMA cantilever will be bent after the deposition due to the tensile stress applied by the reset layer. It will return to its trained flat shape when heated to a temperature greater than A_s. The deformation angle, θ, is determined by the length of the SiO_2 pattern. An arc with a radius, r is formed, which can be expressed as:

$$\frac{1}{r} = \frac{6w_1w_2E_1E_2t_1t_2(t_1+t_2)(\alpha_1-\alpha_2)\Delta T}{(w_1E_1t_1^2)^2+(w_2E_2t_2^2)^2+2w_1w_2E_1E_2t_1t_2(2t_1^2+3t_1t_2+2t_2^2)} \quad (1)$$

where Young's modulus, E; width, w; thickness, t; CTE, α; and temperature, T; and the subscripts 1 and 2 denote NiTi and SiO_2, respectively. However, it is worth noting that this kind of constraint recovery (introducing reset layer to provide mechanical TWSME) could significantly affect the recovery properties (*i.e.*, transition temperature and maximum stress) in contrast with the free recovery (without reset layer) [95,96].

Beside a cantilever type, a novel and unique SMA spiral-coil out-of-plane actuator is reported by Ali *et al.* [97]. The actuator is based on a bulk-micromachined SMA coil with a built-in wireless heater. Compared with the aforementioned actuators where the heating takes place by passing a current into the SMA or by using a heater, the SMA spiral-coil actuator is actuated wirelessly. An AC electromotive force will be generated in the circuit when it is exposed to a radio frequency magnetic field, which has an identical resonant frequency to the LC tank. As a result, AC current flows through the coil and the SMA coil itself produces Joule heat. This approach is promising for the future as it can minimize the actuator's size and complexity.

One of the advantages of using bulk SMA as an actuator is the energy efficiency it provides when strained in pure tension compared to torsion or bending deformations [98]. The strain can be provided by linear or in-plane displacement and can be achieved by using either an SMA tube [99] or SMA wire. Several researchers used an SMA wire directly to provide linear displacement, while some of them realized it by shaping the SMA wire into a spring. By shaping SMA wire into a spring, it can accumulate a small recovery coaxial strain with considerable displacement, which is useful for actuators and measurements [20].

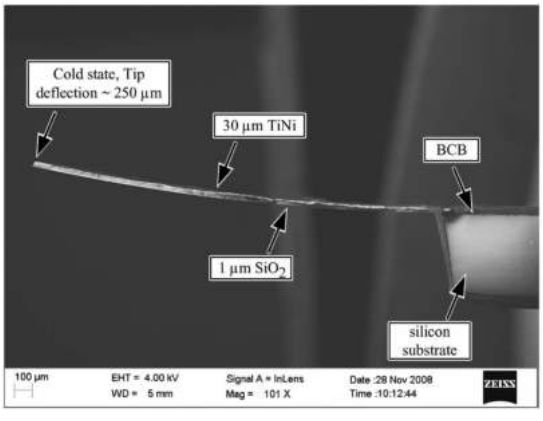

Figure 6. SEM picture of SMA cantilever in cold state. Reprinted with permission from [92], copyright 2009 IEEE.

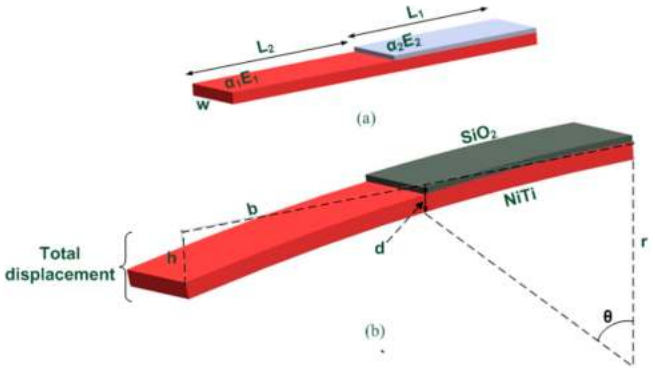

Figure 7. Displacement of cantilever type microactuator using SiO_2 as a reset layer: (**a**) overall structure; (**b**) total displacement after depositing the reset layer.

In terms of applications, several bulk micromachined-SMA actuators have been reported with a variety of mechanisms and actuator structures. In [100], Reynaerts *et al.* report a pincher-like microvalve (Figure 8a). From Figure 8a, it can be seen that the central joint is elastically deformed when the tube is released by contraction of the SMA wire on heating, which provides a simple valve mechanism. Zhao *et al.* [101] report a design and implementation of an SMA nanotweezer actuated at low voltage purposely for nanoscale manipulation. The nanotweezer consists of two electrically controlled SMA actuators provided by two SMA coils that are attached on a fiber-reinforced polymer body to amplify the movement of two tungsten tip end-effectors as shown in Figure 8b. The proposed designs are simpler, easier to control, and operate on lower voltage. Moreover, the SMA actuation utilizes in-plane displacement, which can provide high force actuation. Other than that, Villaneva *et al.* [102] reported a bio-inspired SMA actuator composite (BISMAC) for a robotic jellyfish propulsion system. In [102], the essential structural features of a jellyfish are replicated by the actuator. The actuator is made of silicone, SMA wires, and a steel spring with a simple mechanical structure (Figure 8c). This robotic jellyfish could provide an artificial alternative for the study of jellyfish and allows engineers and scientists to analyze parameters that cannot be analyzed using the actual animal. Clausi *et al.* [103] reported an SMA wires-on-silicon microactuator (Figure 9). The actuator consists of fixed and moveable silicon anchors that are mechanically connected to two SMA wires to form a current loop and silicon cantilevers, which serve as the bias mechanism for reversible motion. Upon heating, strained recovery takes place in the SMA wires, making them contract and bend the cantilevers (Figure 9b). During cooling, part of the elastic energy is released by the cantilevers, which return to their flat position (Figure 9c). The presented method utilizes bulk SMA material in nearly perfect tension, which maximizes the energy efficiency.

An interesting micro-rotary actuator is shown by Gabriel *et al.* [104] using 100 μm wire of NiTi SMA. In [104], the wire is clamped at both ends under torsional strain. The actuation is performed by connecting electrical connections (two at each ends and one in the middle of the wire), which are heated separately (Figure 10a). This enables repeatable, continuous, and directional angular deflections of the wire about its longitudinal axis, which provides a unique actuation scheme. A multi-directional tubular micro-manipulator fabricated from a NiTiCu SMA tube is reported by Mineta *et al.* [105,106]. Three meandering actuators are fabricated from an SMA tube. Each meander can be heated individually, which results in multi-directional displacement actuation (Figure 10b). With controllable bending motion function, the micro-manipulator can be used as an active catheter for interventional diagnosis and therapy.

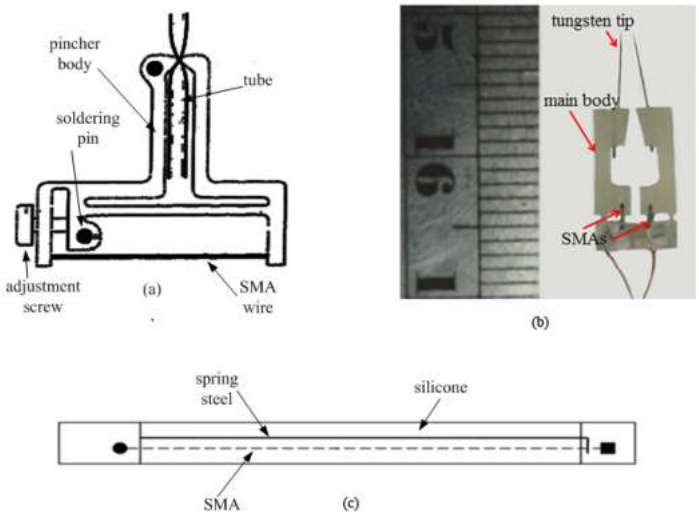

Figure 8. (**a**) Concept of a pincher-like shape memory actuated microvalve. Reprinted with permission from [100], copyright 1997 Elsevier. (**b**) Actual photo of a nanotweezer fabricated by Zhao et al. Reprinted with permission from [101], copyright 2014 Institute of Physics. (**c**) Schematic of a BISMAC actuator. Reprinted with permission from [102], copyright 2011 Institute of Physics.

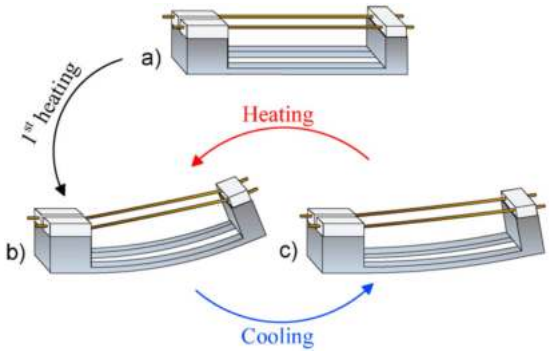

Figure 9. Operational states of microactuator design and fabrication by Clausi *et al*. Reprinted with permission from [103], copyright 2013 Elsevier.

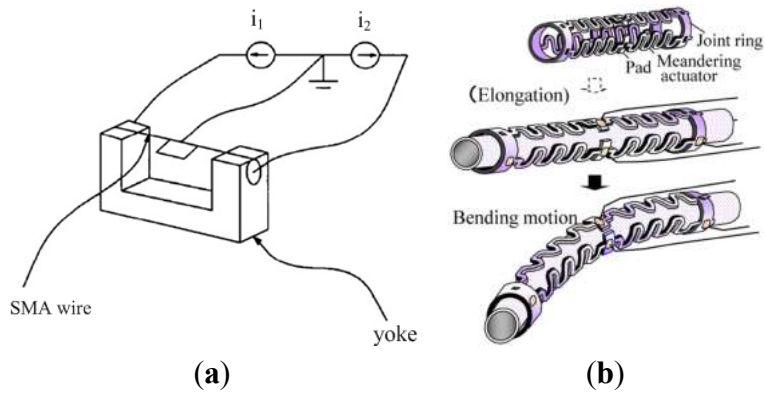

Figure 10. (**a**) Diagram of a micro-rotary actuator showing the clamping yoke, torsionally strained SMA wire, and electronic SMA actuator. Reprinted with permission from [104], copyright 1998 Elsevier. (**b**) The concept of tube-shaped SMA. Reprinted with permission from [105], copyright 2011 Elsevier.

5. Micromechanism Device for Biomedical Applications

Practical applications of SMA in medicine are seen particularly in vascular medicine [107–111], dentistry [112,113], orthopedics [114–116], and other related areas [117–120]. In this section, the application of SMA actuators in the biomedical field is presented. One of the most beneficial applications of MEMs in biomedicine is the microgripper. Apart from the manipulation of microscopic objects in factory automation and assembly, it can also be applied for handling biological cells as well as in robot-assisted surgery. The most common gripper jaw design is based on two cantilever beams spaced out by a certain distance, as illustrated in Figure 11a. In Figure 11a, the tip of one side of both cantilevers is actuated, making the tip close or open and hence grasp or release an object depending on the actuator scheme.

One of the earliest reports on the SMA cantilever-type microgripper design was published by Lee *et al.* [121] in 1996. In [121], the microgripper is actuated by NiTiCu thin-film SMA deposited on a silicone cantilever beam, which acts as a bias spring. The transformation temperature is 37 °C, which is near to human body temperature, making it useful for medical applications. In [122], Huang *et al.* introduced a simple processing technique and batch friendly for the fabrication of a cantilever type microgripper (Figure 11a). The design is basically similar to the microgripper fabricated by Lee *et al.* [121], in which NiTi thin-film SMA was deposited on Si wafer. Both microgrippers mentioned above are actuated by means of thin-film SMA, which has disadvantages such as a thin-film deposition consistency and relatively low actuation force compared to that of bulk SMA. The bulk SMA could be used instead to overcome these shortcomings.

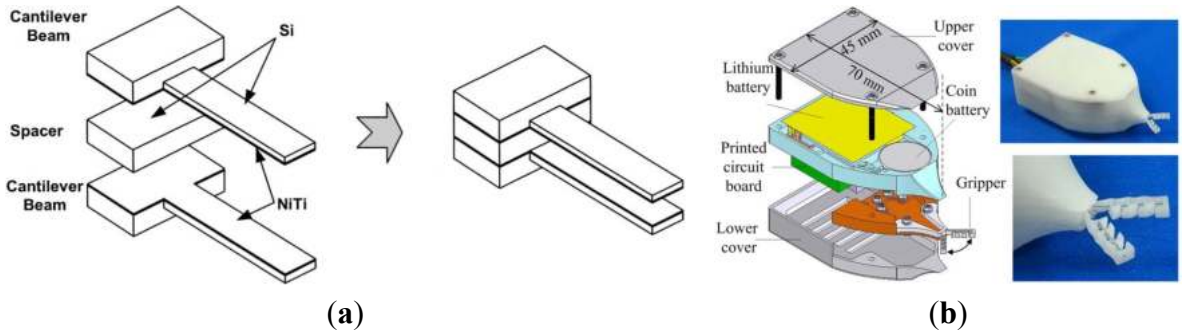

Figure 11. (**a**) Illustration of gripper assembly by Huang *et al.* Reprinted with permission from [122], copyright 2003 SPIE. (**b**) Self-sensing microgripper module by Lan *et al.* Reprinted with permission from [123], copyright 2011 IEEE.

Among the well-known microgrippers fabricated using bulk SMA is the polymer-based microgripper cantilever reported by Houston *et al.* [124]. The cantilever is actuated by an SMA wire embedded in the microgripper during molding of polyurethane. Since there is no direct physical contact of SMA with the body, this type of microgripper is preferable in medical surgery. With this configuration, the object temperature has a limited influence on the SMA temperature and is extremely useful for biomedical applications.

Although the aforementioned microgrippers show excellent potential in various applications, they do not have the capability to control the gripping level once they are actuated. Hence, the grasped object can be damaged if excessive force is applied. It is necessary for the microgripper to be equipped

with a force sensor in order to overcome this problem, especially when handling living cells or in any other sensitive biomedical applications. For this reason, Lan *et al.* [123] reported extensively on a compliant two-fingered microgripper, which mimics human finger actuation, as shown in Figure 11b. In [123], the contraction force is estimated by the force-resistance relationship of the SMA wire. Despite this advantage, the microgripper requires extra circuitry for resistance feedback control to obtain the desired contraction force. Moreover, this system tends to be complex and large due to the use of batteries or electronic circuitry for its operation. To overcome this problem, a passive approach for SMA actuation using RF is presented by Ali *et al.* [19]. Similarly to their previous work in [97], the microgripper is operated through an LC resonant circuit serving as a frequency-sensitive wireless heater. The heater is activated by an external RF magnetic field. The microgripper, as shown in Figure 12, consists of two beams fabricated by bulk micromachining of the SMA sheet, where SiO_2 is used as the bias spring. Both cantilever and heater are bonded by electroplated copper. The proposed wireless microgripper is promising for wireless capsule endoscopy, where it could serve as a biopsy jaw. However, the heating efficiency could deteriorate since no heat insulation exists between the SMA and the environment. An aerogel that has a very low thermal conductivity has the potential to address this issue, where it can be coated around the SMA and heater circuit.

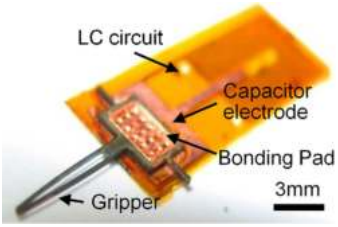

Figure 12. Overall shape of frequency controller microgripper by Ali *et al*. Reprinted with permission from [19], copyright 2010 Elsevier.

Beside the microgripper, a MEMS reservoir based drug delivery system could make a significant contribution to targeted drug delivery mechanisms by incorporating features such as control over the drug delivery rate, a programmable drug schedule, and the ability to reach difficult treatment locations. This parallels with Paul Ehrlich's proposed concept of a 'magic bullet', which suggest the benefit of targeted delivery drug to the diseased cell. Such a drug delivery system is composed of at least a reservoir for the drug, the microvalve, and/or the micropump. The first SMA micropump was reported in 1998 by Bernard *et al.* [87]. The reciprocating pumps consist of a deformable chamber and two check valves (Figure 13a). Polyimide is used as a spring bias. Besides providing the spring biased, the polyimide also isolates the NiTi in the actuator from the fluid both thermally and chemically. By doing so, the risk of thermal coupling and chemical reaction between the fluid and NiTi thin-film is removed or at least reduced. Xu *et al.* [88] later reported a novel diaphragm-actuated micropump by using a thin-film NiTi/Si bimorph structure (Figure 13b). Compared with the micropump proposed by Bernard, no special bias structure is required as the silicon substrate itself provides the biasing force. Moreover, the silicon can provide isolation from the working liquid and NiTi. The proposed pump has a greater flow rate and driving frequency than the polyimide spring biased proposed by Bernard. Makino *et al.* [89] proposed another thin-film SMA-based micropump for drug-delivery applications using pressurized gas as the biasing mechanism. NiTi film and a Pyrex glass cap with a square recess are anodically bonded together

in a vacuum to form a chamber. Then a bias pressure is applied to deform the NiTi thin-film. When the diaphragm is heated, its initial flat shape is recovered, making the pumping chamber contract, and hence liquid is sucked in. When the diaphragm cools, the liquid is pumped out and deformed due to the biased pressure. The pump configuration and working illustration are as shown in Figure 14. By using the bias pressure method, the structure of the micropump becomes simpler compared to other methods. Moreover, the pumping pressure can be conveniently controlled merely by changing the bias pressure.

When dealing with SMA actuators, particularly in biomedical applications, the main issue is the actuation temperature. Small hysteresis SMA is always desired to improve the efficiency with low-temperature actuation. Low hysteresis is also used to increase the pumping frequency, which is important to improve the flow rate. The addition of a ternary element in binary NiTi SMA is known for having an impact on the SMA hysteresis. For this reason, Zhang *et al.* [125] proposed the use of a $Ni_{41.1at\%}Ti_{50.7}Cu_{8.2}$ thin-film SMA micropump. Based on their results, the micropump as less hysteresis (9 °C) compared to all the aforementioned pumps. Furthermore, the highest pumping frequency attained is 100 Hz, and more than 200,000 driving cycles are achieved without any drift in the diaphragm displacement.

Attempts to fabricate a peristaltic-type micropump using SMA have also been observed over the years. A peristaltic micropump does not have moving parts and thus avoids particles or living cells becoming damaged or stuck [126]. Therefore, it is a suitable candidate for blood transportation applications. Unlike micropumps that utilize a check valve applied in the reciprocating micropump, in peristaltic pumps, a simpler design and fabrication process are involved [127]. Gu *et al.* [128] reported a peristaltic micropump consisting of twelve SMA springs, four latex tubes, three coupled extrusion poles, and two one-way valves installed one on each side of the pump chamber as shown in Figure 15a. Because of the larger SMA dimensions and number of actuators used, the pump was able to provide the highest flow rate of 1000 μL/min. A smaller scale for this type of micropump was reported by Shkolnikov *et al.* [129] in 2010. The SMA wire actuated pump is shown schematically in Figure 15b. The SMA micropump design achieved five-fold package volume and four-fold weight reductions compared to the electrical motor design mentioned in the same report. Moreover, the operating pressure is higher than its electrical motor driven counter part. Table 2 shows a comparison of the SMA-based micropumps reported by the different authors mentioned above. The performance characteristics and key features of the micropumps are also summarized.

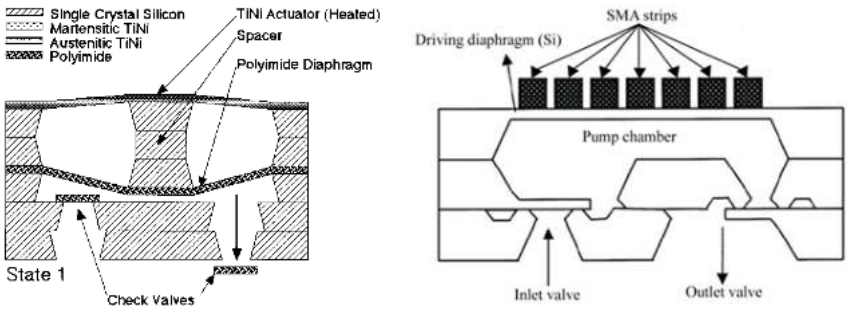

(**a**) (**b**)

Figure 13. (**a**) Polyimide spring-biased actuator micropump by Bernard *et al.* [87]. Reprinted with permission from [87], copyright 1998 IEEE. (**b**) NiTi/Si bimorph actuated micropump structure by Xu *et al.* Reprinted with permission from [88], copyright 2001 Elsevier.

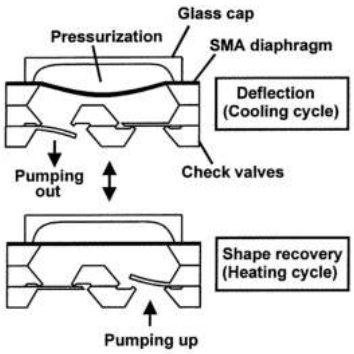

Figure 14. Pressurized spring-biased actuator micropump structure with SMA actuator. Reprinted with permission from [89], copyright 2001 Elsevier.

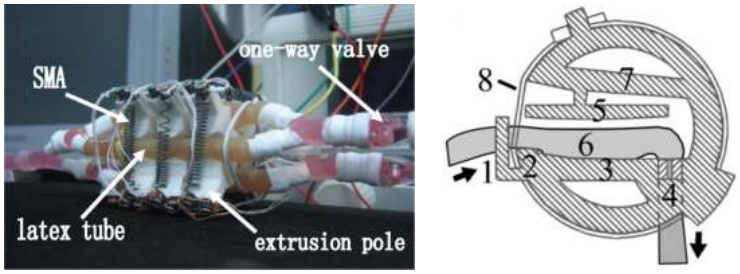

(**a**) (**b**)

Figure 15. (**a**) Peristaltic micropump by Guo *et al.* Reprinted with permission from [128], copyright 2008 IEEE. (**b**) SMA wire actuated peristaltic micropump by Shkolnikov *et al.* Black arrows represent the flow direction: 1, pre-constriction; 2, upstream valve; 3, base; 4, downstream valve; 5, plunger; 6, pumping chamber (flexible tube); 7, plunger arm; and 8, SMA wire (actuator). Reprinted with permission from [129], copyright 2010 Elsevier.

Table 2. SMA actuated micropumps.

References	Pump Type	Size	SMA Form	Bias Type	Highest Flowrate (μL/min)	Highest Frequency (Hz)	Diaphragm Displacement
[87]	Reciprocal	n/r	Thin-film	Polyimide	6 at 0.8 Hz	1.2	n/r
[87]	Reciprocal	n/r	Thin-film	Antagonistic	50 at 0.9 Hz	1.1	80 μm
[88]	Reciprocal	6 mm × 6 mm × 1.5 mm	Thin-film	NiTi/Si bimorph	340 at 60 Hz	100	5 μm
[89]	Reciprocal	10 mm × 20 mm × 1.4 mm	Thin-film	Pressurization	4.8 at 0.5 Hz	0.5	95 μm
[125]	Reciprocal	8 mm × 8 mm × 1.8 mm	Thin-film	NiTiCu/Si bimorph	235 at 80 Hz	100	6 μm
[130]	Reciprocal	16 mm × 74 mm	Coil	TWSME	700 at 2.0 Hz	10	10 mm
[131]	Reciprocal	n/r	Coil	Antagonistic	n/r	n/r	n/r
[128]	Peristaltic	45 mm × 30 mm × 30 mm	Coil	Antagonistic	1000 at 0.6 Hz	50	8 mm
[129]	Peristaltic	1.3 cm^3	Wire	TWSME	60	n/r	n/r

6. Conclusions

In this paper, the fabrication of thin-films and manufacture of bulk SMA was presented. The most common method used to deposit thin-film SMA is sputtering deposition. Other methods include flash evaporation, pulsed laser deposition, filtered arc deposition, cluster beam deposition, and cathodic arc

plasma ion plating. It was shown that Ti-rich films exhibit a transformation temperature near to or above ambient temperature. The casting methods that are widely used for bulk SMA manufacture are the VIM, VAR, and EBM processes and their advantages and disadvantages are described. The actuator schemes used are diaphragm and cantilever actuators, which provide out-of-plane actuation. An in-plane displacement can be achieved by using an SMA tube, wire, or spring. Microgrippers and micropumps are among the favorable usages of SMA for applications in biomedicine.

Acknowledgments

The authors acknowledge the financial support from Ministry of Science, Technology and Innovation Malaysia under E-science Fund and Ministry of Education Malaysia (MOE) under PRGS and FRGS schemes. Mohamad Amri acknowledges the financial support from Universiti Teknologi Malaysia (UTM) under Zamalah scheme.

Conflicts of Interest

The authors declare no conflict of interest.

References

1. Sun, L.; Huang, W.M.; Ding, Z.; Zhao, Y.; Wang, C.C.; Purnawali, H.; Tang, C. Stimulus-responsive shape memory materials: A review. *Mater. Des.* **2012**, *33*, 577–640.
2. Huang, W.M.; Ding, Z.; Wang, C.C.; Wei, J.; Zhao, Y.; Purnawali, H. Shape memory materials. *Mater. Today* **2010**, *13*, 54–61.
3. Otsuka, K.; Kakeshita, T. Science and technology of shape-memory alloys: New developments. *MRS Bull.* **2002**, *27*, 91–98.
4. Kudva, J.N. Overview of the DARPA Smart Wing Project. *J. Intell. Mater. Syst. Struct.* **2004**, *15*, 261–267.
5. Dunne, J.; Pitt, D.; White, E.; Garcia, E. Ground demonstration of the Smart Inlet. In Proceedings of the 41st Structures, Structural Dynamics, and Materials Conference, Atlanta, GA, USA, 3–6 April 2000.
6. Petrini, L.; Migliavacca, F. Biomedical Applications of Shape Memory Alloys. *J. Metall.* **2011**, *2011*, 1–15.
7. Small, W., IV; Wilson, T.S.; Buckley, P.R.; Benett, W.J.; Loge, J.M.; Hartman, J.; Maitland, D.J. Prototype fabrication and preliminary *in vitro* testing of a shape memory endovascular thrombectomy device. *IEEE Trans. Biomed. Eng.* **2007**, *54*, 1657–1666.
8. Haga, Y.; Mizushima, M.; Matsunaga, T.; Esashi, M. Medical and welfare applications of shape memory alloy microcoil actuators. *Smart Mater. Struct.* **2005**, *14*, S266–S272.
9. Bossi, S.; Kammer, S.; Dörge, T.; Menciassi, A.; Hoffmann, K.P.; Micera, S. An implantable microactuated intrafascicular electrode for peripheral nerves. *IEEE Trans. Biomed. Eng.* **2009**, *56*, 2701–2706.
10. Murad, S.; Murad, J.; Khan, H. A smarter SMA technology for the realization of drug delivering endoscopic capsule. *Rawal Med. J.* **2013**, *38*, 66–74.

11. Miyazaki, S.; Kim, H.Y.; Hosoda, H. Development and characterization of Ni-free Ti-base shape memory and superelastic alloys. *Mater. Sci. Eng. A* **2006**, *438–440*, 18–24.
12. McMahon, R.E.; Ma, J.; Verkhoturov, S.V.; Munoz-Pinto, D.; Karaman, I.; Rubitschek, F.; Maier, H.J.; Hahn, M.S. A comparative study of the cytotoxicity and corrosion resistance of nickel-titanium and titanium-niobium shape memory alloys. *Acta Biomater.* **2012**, *8*, 2863–2870.
13. Farooq, M.U.; Khalid, F.A.; Zaigham, H.; Abidi, I.H. Superelastic behaviour of Ti-Nb-Al ternary shape memory alloys for biomedical applications. *Mater. Lett.* **2014**, *121*, 58–61.
14. Lai, M.; Gao, Y.; Yuan, B.; Zhu, M. Effect of Pore Structure Regulation on the Properties of Porous TiNbZr Shape Memory Alloys for Biomedical Application. *J. Mater. Eng. Perform.* **2015**, *24*, 136–142.
15. Ijaz, M.F.; Kim, H.Y.; Hosoda, H.; Miyazaki, S. Superelastic properties of biomedical (Ti-Zr)-Mo-Sn alloys. *Mater. Sci. Eng. C* **2015**, *48*, 11–20.
16. Surbled, P.; Clerc, C.; le Pioufle, B.; Ataka, M.; Fujita, H. Effect of the composition and thermal annealing on the transformation temperatures of sputtered TiNi shape memory alloy thin films. *Thin Solid Films* **2001**, *401*, 52–59.
17. Sandström, N.; Braun, S.; Stemme, G.; van der Wijngaart, W.; Royal, K.T.H. Full Wafer Integration of Shape Memory Alloy Microactuators Using Adhesive Bonding. In Proceedings of the Transducer 2009, International Solid-State Sensors, Actuators and Microsystems Conference, Denver, CO, USA, 21–25 June 2009; pp. 845–848.
18. Biffi, C.A.; Nespoli, A.; Previtali, B.; Villa, E.; Tuissi, A. Functional Response of NiTi Elements for Smart Micro-actuation Applications. *J. Mater. Eng. Perform.* **2014**, *23*, 2351–2356.
19. Mohamed Ali, M.S.; Takahata, K. Frequency-controlled wireless shape-memory-alloy microactuators integrated using an electroplating bonding process. *Sens. Actuators A Phys.* **2010**, *163*, 363–372.
20. Wang, J. Shape memory effect of TiNi-based springs trained by constraint annealing. *Met. Mater. Int.* **2013**, *19*, 295–301.
21. Walker, J.A.; Gabriel, K.J.; Mehregany, M. Thin-film processing of TiNi shape memory alloy. *Sens. Actuators A Phys.* **1990**, *21*, 243–246.
22. Roch, I.; Bidaud, P.; Collard, D.; Buchaillot, L. Fabrication and characterization of an SU-8 gripper actuated by a SMA thin film. *J. Micromech. Microeng.* **2003**, *13*, 330.
23. Gill, J.J.; Ho, K.; Carman, G.P. Three-dimensional thin-film shape memory alloy microactuator with two-way effect. *J. Microelectromech. Syst.* **2002**, *11*, 68–77.
24. Zhang, H.; Qiu, C. Characteristic of TiNi(Cu) shape memory thin film based on micropump. In Proceedings of the 2nd International Conference on Smart Materials and Nanotechnology in Engineering, Weihai, China, 8–11 July 2009.
25. Kuribayashi, K. Micro SMA actuator and motion control. In Proceedings of the 2000 International Symphosium on Micromechatronics and Human Science, Nagoya, Japan, 22–25 October 2000; pp. 35–42.
26. Tomozawa, M.; Kim, H.Y.; Miyazaki, S. Microactuators Using R-phase Transformation of Sputter-deposited Ti-47.3Ni Shape Memory Alloy Thin Films. *J. Intell. Mater. Syst. Struct.* **2006**, *17*, 1049–1058.

27. Bhattacharya, R.S.; Rai, A.K.; Pronko, P.P. Corrosion behavior of amorphous TiNi films fabricated by ion beam mixing. *Mater. Lett.* **1984**, *2*, 483–486.
28. Makino, E.; Uenoyama, M.; Shibata, T. Flash evaporation of TiNi shape memory thin film for microactuators. *Sens. Actuators A Phys.* **1998**, *71*, 187–192.
29. Adams, T.M.; Kirkpatrick, S.R.; Wang, Z.; Siahmakoun, A. NiTi shape memory alloy thin films deposited by co-evaporation. *Mater. Lett.* **2005**, *59*, 1161–1164.
30. Chen, X.; Lu, Y.; Ren, Z.; Zhu, S. The fabrication of TiNi thin films by pulsed-laser deposition. *Proc. SPIE* **2002**, *4426*, 225–228.
31. Cha, J.O.; Nam, T.H.; Alghusun, M.; Ahn, J.S. Composition and crystalline properties of TiNi thin films prepared by pulsed laser deposition under vacuum and in ambient Ar gas. *Nanoscale Res. Lett.* **2012**, *7*, 1–15.
32. Ahn, J.S.; Cha, J.O.; Shin, C.H.; Yeo, S.J.; Im, H.J.; Sakai, J.; Lee, K.B.; Kim, H.M.; Nam, T.H. Effect of ambient Ar gas on the composition control and crystalline properties of TiNi thin films fabricated by using pulsed laser deposition. *J. Korean Phys. Soc.* **2007**, *50*, 1750–1754.
33. Chen, X.Y.; Lu, Y.F.; Ren, Z.M.; Zhu, S. Fabrication of TiNi shape memory alloy thin films by pulsed-laser deposition. *J. Mater. Res.* **2002**, *17*, 279–283.
34. Ciabattari, F.; Fuso, F.; Arimondo, E. Pulsed laser deposition of NiTi shape memory effect thin films. *Appl. Phys. A Mater. Sci. Process.* **1998**, *64*, 623–626.
35. Yang, L.M.; Tieu, A.K.; Dunne, D.P.; Huang, S.W.; Li, H.J.; Wexler, D.; Jiang, Z.Y. Cavitation erosion resistance of NiTi thin films produced by Filtered Arc Deposition. *Wear* **2009**, *267*, 233–243.
36. Barborini, E.; Piseri, P.; Mutti, S.; Milani, P.; Biasioli, F.; Iannotta, S.; Gialanella, S. Synthesis of nanocrystalline TiNi thin films by cluster beam deposition. *Nanostruct. Mater.* **1998**, *10*, 1023–1031.
37. He, J.L.; Won, K.W.; Chang, J.T. TiNi thin films prepared by cathodic arc plasma ion plating. *Thin Solid Films* **2000**, *359*, 46–54.
38. Ishida, A. Progress in thin-film shape-memory-alloy actuators. In Proceedings of the 17th International Conference on Solid-State Sensors, Actuators and Microsystems (TRANSDUCERS and EUROSENSORS XXVII), Barcelona, Spain, 16–20 June 2013; pp. 1573–1578.
39. Reichelt, K.; Jiang, X. The preparation of thin films by physical vapour deposition methods. *Thin Solid Films* **1990**, *191*, 91–126.
40. Boyd, A.R.; O'Kane, C.; Meenan, B.J. Control of calcium phosphate thin film stoichiometry using multi-target sputter deposition. *Surf. Coat. Technol.* **2013**, *233*, 131–139.
41. Schell, N.; Martins, R.M.S.; Braz Fernandes, F.M. Real-time and in-situ structural design of functional NiTi SMA thin films. *Appl. Phys. A Mater. Sci. Process.* **2005**, *81*, 1441–1445.
42. Kabla, M.; Seiner, H.; Musilova, M.; Landa, M.; Shilo, D. The relationships between sputter deposition conditions, grain size, and phase transformation temperatures in NiTi thin films. *Acta Mater.* **2014**, *70*, 79–91.
43. Ho, K.K.; Carman, G.P. Sputter deposition of NiTi thin film shape memory alloy using a heated target. *Thin Solid Films* **2000**, *370*, 18–29.
44. Kim, S.-W.; Jeon, Y.M.; Park, C.H.; Kim, J.H.; Kim, D.-H.; Yeom, J.-T. Martensitic phase transformation of TiNi thin films fabricated by co-sputtering deposition. *J. Alloys Compd.* **2013**, *580*, 5–9.

45. Huang, X.; Liu, Y. Surface morphology of sputtered NiTi-based shape memory alloy thin films. *Surf. Coat. Technol.* **2005**, *190*, 400–405.
46. Huang, X.; Liu, Y. Some factors affecting the properties of sputter deposited NiTi-based shape memory alloy thin films. *Proc. SPIE* **2002**, *4934*, 210–218.
47. Tang, W.; Sundman, B.; Sandström, R.; Qiu, C. New modelling of the B2 phase and its associated martensitic transformation in the Ti-Ni system. *Acta Mater.* **1999**, *47*, 3457–3468.
48. Bendahan, M.; Seguin, J.-L.; Canet, P.; Carchano, H. NiTi shape memory alloy thin films: Composition control using optical emission spectroscopy. *Thin Solid Films* **1996**, *283*, 61–66.
49. Chun, Y.J.; Levi, D.S.; Mohanchandra, K.P.; Fishbein, M.C.; Carman, G.P. Novel micro-patterning processes for thin film NiTi vascular devices. *Smart Mater. Struct.* **2010**, *19*, 105021.
50. Sanjabi, S.; Naderi, M.; Zare Bidaki, H.; Sadrnezhaad, S.K.; Bidaki, H.Z. Characterization of sputtered NiTi shape memory alloy thin films. *Sci. Iran.* **2009**, *16*, 248–252.
51. Liu, Y.S.; Xu, D.; Jiang, B.H.; Yuan, Z.Y.; van Houtte, P. The effect of crystallizing procedure on microstructure and characteristics of sputter-deposited TiNi shape memory thin films. *J. Micromech. Microeng.* **2005**, *15*, 575–579.
52. Mohanchandra, K.P.; Ho, K.K.; Carman, G.P. Compositional uniformity in sputter-deposited NiTi shape memory alloy thin films. *Mater. Lett.* **2008**, *62*, 3481–3483.
53. Fu, Y.; Du, H.; Huang, W.; Zhang, S.; Hu, M. TiNi-based thin films in MEMS applications: A review. *Sens. Actuators A Phys.* **2004**, *112*, 395–408.
54. Cole, D.; Bruck, H.; Roytburd, A. Nanomechanical characterization of diffusion-modified graded NiTi films. In Proceedings of the 11th International Congress and Exhibition on Experimental and Applied Mechanics, Orlando, FL, USA, 2–5 June 2008; pp. 1722–1728.
55. Martins, R.M.S.; Schell, N.; Reuther, H.; Pereira, L.; Mahesh, K.K.; Silva, R.J.C.; Fernandes, F.M.B. Texture development, microstructure and phase transformation characteristics of sputtered Ni-Ti Shape Memory Alloy films grown on TiN<111>. *Thin Solid Films* **2010**, *519*, 122–128.
56. Martins, R.M.S.; Schell, N.; Mahesh, K.K.; Silva, R.J.C.; Fernandes, F.M.B. X-ray diffraction studies during magnetron co-sputtering of Ni-Ti shape memory alloy films. *Ciênc. Tecnol. Mater.* **2012**, *24*, 161–169.
57. Sato, M.; Ishida, A.; Miyazaki, S. Two-Way shape memory effect of sputter-deposited thin films of Ti 51.3 at.% Ni. *Thin Solid Films* **1998**, *315*, 305–309.
58. He, Q.; Hong, M.H.; Huang, W.M.; Chong, T.C.; Fu, Y.Q.; Du, H.J. CO_2 laser annealing of sputtering deposited NiTi shape memory thin films. *J. Micromech. Microeng.* **2004**, *14*, 950–956.
59. Sadrnezhaad, S.K.; Rezvani, E.; Sanjabi, S.; Ziaei Moayed, A.A. Pulsed-laser annealing of NiTi shape memory alloy thin film. *J. Mater. Sci. Technol.* **2009**, *25*, 135–140.
60. Bellouard, Y.; Lehnert, T.; Bidaux, J.-E.; Sidler, T.; Clavel, R.; Gotthardt, R. Local annealing of complex mechanical devices: A new approach for developing monolithic micro-devices. *Mater. Sci. Eng. A* **1999**, *273–275*, 795–798.
61. Frenzel, J.; Zhang, Z.; Somsen, C.; Neuking, K.; Eggeler, G. Influence of carbon on martensitic phase transformations in NiTi shape memory alloys. *Acta Mater.* **2007**, *55*, 1331–1341.
62. Frenzel, J.; Zhang, Z.; Neuking, K.; Eggeler, G. High quality vacuum induction melting of small quantities of NiTi shape memory alloys in graphite crucibles. *J. Alloys Compd.* **2004**, *385*, 214–223.

63. Nayan, N.; Govind; Saikrishna, C.N.; Ramaiah, K.V.; Bhaumik, S.K.; Nair, K.S.; Mittal, M.C. Vacuum induction melting of NiTi shape memory alloys in graphite crucible. *Mater. Sci. Eng. A* **2007**, *465*, 44–48.
64. Kabiri, Y.; Kermanpur, A.; Foroozmehr, A. Comparative study on microstructure and homogeneity of NiTi shape memory alloy produced by copper boat induction melting and conventional vacuum arc melting. *Vacuum* **2012**, *86*, 1073–1077.
65. Frenzel, J.; George, E.P.; Dlouhy, A.; Somsen, C.; Wagner, M.F.-X.; Eggeler, G. Influence of Ni on martensitic phase transformations in NiTi shape memory alloys. *Acta Mater.* **2010**, *58*, 3444–3458.
66. Lin, H.C.; Wu, S.K. Effects of hot rolling on the martensitic transformation of an equiatomic TiNi alloy. *Mater. Sci. Eng. A* **1992**, *158*, 87–91.
67. Shahmir, H.; Nili-Ahmadabadi, M.; Naghdi, F. Superelastic behavior of aged and thermomechanical treated NiTi alloy at A_f+10 °C. *Mater. Des.* **2011**, *32*, 365–370.
68. Otubo, J.; Rigo, O.D.; Neto, C.M.; Mei, P.R. The effects of vacuum induction melting and electron beam melting techniques on the purity of NiTi shape memory alloys. *Mater. Sci. Eng. A* **2006**, *438–440*, 679–682.
69. Huang, W.; Goh, H.B. On the long-term stability of two-way shape memory alloy trained by reheat treatment. *J. Mater. Sci. Lett.* **2001**, *20*, 1795–1797.
70. Huang, W.M.; Goh, H.B.; Li, C. Effects of reheat treatment conditions on two-way shape memory. *J. Mater. Sci. Lett.* **2002**, *21*, 991–993.
71. Huang, W.; Toh, W. Training two-way shape memory alloy by reheat treatment. *J. Mater. Sci. Lett.* **2000**, *19*, 1549–1550.
72. Chang, C.-Y.; Vokoun, D.; Hu, C.-T. Two-way shape memory effect of NiTi alloy induced by constraint aging treatment at room temperature. *Metall. Mater. Trans. A Phys. Metall. Mater. Sci.* **2001**, *32*, 1629–1634.
73. Wada, K.; Liu, Y. On the two-way shape memory behavior in NiTi alloy-An experimental analysis. *Acta Mater.* **2008**, *56*, 3266–3277.
74. Costanza, G.; Tata, M.E.; Calisti, C. Nitinol one-way shape memory springs: Thermomechanical characterization and actuator design. *Sens. Actuators A Phys.* **2010**, *157*, 113–117.
75. Lahoz, R.; Puértolas, J.A. Training and two-way shape memory in NiTi alloys: Influence on thermal parameters. *J. Alloys Compd.* **2004**, *381*, 130–136.
76. Kato, T.; Tokuda, M.; Inaba, T.; Yamazaki, M. Experimental research on two-way shape memory effect of TiNi shape memory alloy. *Key Eng. Mater.* **2004**, *274–276*, 1095–1100.
77. Wada, K.; Liu, Y. Thermomechanical training and the shape recovery characteristics of NiTi alloys. *Mater. Sci. Eng. A* **2008**, *481–482*, 166–169.
78. Kim, H.-C.; Yoo, Y.-I.; Lee, J.-J. Development of a NiTi actuator using a two-way shape memory effect induced by compressive loading cycles. *Sens. Actuators A Phys.* **2008**, *148*, 437–442.
79. Yoo, Y.I.; Lee, J.J. Two-way shape memory effect of NiTi under compressive loading cycles. *Phys. Procedia* **2011**, *22*, 449–454.
80. Yoo, Y.I.; Jeong, J.W.; Lee, J.J.; Lee, C.H. Effect of heat treatment on the two-way recovery stress of tube-shaped NiTi. *J. Intell. Mater. Syst. Struct.* **2012**, *23*, 1161–1168.
81. Behl, M.; Lendlein, A. Triple-Shape polymers. *J. Mater. Chem.* **2010**, *20*, 3335–3345.

82. Wei, M.; Zhan, M.; Yu, D.; Xie, H.; He, M.; Yang, K.; Wang, Y. Novel poly(tetramethylene ether)glycol and poly(ε-caprolactone) based dynamic network via quadruple hydrogen bonding with triple-shape effect and self-healing capacity. *ACS Appl. Mater. Interfaces* **2015**, *7*, 2585–2596.
83. Nejad, H.B.; Baker, R.M.; Mather, P.T. Preparation and characterization of triple shape memory composite foams. *Soft Matter* **2014**, *10*, 8066–8074.
84. Chatani, S.; Wang, C.; Podgórski, M.; Bowman, C.N. Triple shape memory materials incorporating two distinct polymer networks formed by selective thiol-Michael addition reactions. *Macromolecules* **2014**, *47*, 4949–4954.
85. Tang, C.; Huang, W.M.; Wang, C.C.; Purnawali, H. The triple-shape memory effect in NiTi shape memory alloys. *Smart Mater. Struct.* **2012**, *21*, 085022.
86. Nisar, A.; Afzulpurkar, N.; Mahaisavariya, B.; Tuantranont, A. MEMS-Based micropumps in drug delivery and biomedical applications. *Sens. Actuators B Chem.* **2008**, *130*, 917–942.
87. Benard, W.L.; Kahn, H.; Heuer, A.H.; Huff, M.A. Thin-film shape-memory alloy actuated micropumps. *J. Microelectromech. Syst.* **1998**, *7*, 245–251.
88. Xu, D.; Wang, L.; Ding, G.; Zhou, Y.; Yu, A.; Cai, B. Characteristics and fabrication of NiTi/Si diaphragm micropump. *Sens. Actuators A Phys.* **2001**, *93*, 87–92.
89. Makino, E.; Mitsuya, T.; Shibata, T. Fabrication of TiNi shape memory micropump. *Sens. Actuators A Phys.* **2001**, *88*, 256–262.
90. Shin, D.D.; Mohanchandra, K.P.; Carman, G.P. Development of hydraulic linear actuator using thin film SMA. *Sens. Actuators A Phys.* **2005**, *119*, 151–156.
91. Wongweerayoot, E.; Srituravanich, W.; Pimpin, A. Fabrication and Characterization of Nitinol-Copper Shape Memory Alloy Bimorph Actuators. *J. Mater. Eng. Perform.* **2014**, *24*, 635–643.
92. Braun, S.; Sandstrom, N.; Stemme, G.; van der Wijngaart, W. Wafer-scale manufacturing of bulk shape-memory-alloy microactuators based on adhesive bonding of titanium-nickel sheets to structured silicon wafers. *J. Microelectromech. Syst.* **2009**, *18*, 1309–1317.
93. Mohamed Ali, M.S.; Takahata, K. Wireless microfluidic control with integrated shape-memory-alloy actuators operated by field frequency modulation. *J. Micromech. Microeng.* **2011**, *21*, 075005.
94. Dahmardeh, M.; Mohamed Ali, M.S.; Saleh, T.; Hian, T.M.; Moghaddam, M.V.; Nojeh, A.; Takahata, K. High-power MEMS switch enabled by carbon-nanotube contact and shape-memory-alloy actuator. *Phys. Status Solidi* **2013**, *210*, 631–638.
95. Li, Y.F.; Mi, X.J.; Yin, X.Q.; Xie, H.F. Constrained recovery properties of NiTi shape memory alloy wire during thermal cycling. *J. Alloys Compd.* **2014**, *588*, 525–529.
96. Pan, G.H.; Huang, W.M. A note on constrained shape memory alloys upon thermal cycling. *J. Mater. Sci.* **2006**, *41*, 7964–7968.
97. Mohamed Ali, M.S.; Ali, M.; Bycraft, B.; Bsoul, A.; Takahata, K. Radio-controlled microactuator based on shape-memory-alloy spiral-coil inductor. *J. Microelectromech. Syst.* **2013**, *22*, 331–338.
98. Reynaerts, D.; van Brussel, H. Design aspects of shape memory actuators. *Mechatronics* **1998**, *8*, 635–656.
99. Yoo, Y.I.; Lee, J.J.; Lee, C.H.; Lim, J.H. An experimental study of the two-way shape memory effect in a NiTi tubular actuator. *Smart Mater. Struct.* **2010**, *19*, 125002.

100. Reynaerts, D.; Peirs, J.; van Brussel, H. An implantable drug-delivery system based on shape memory alloy micro-actuation. *Sens. Actuators A Phys.* **1997**, *61*, 455–462.
101. Zhao, H.; Chang, M.; Liu, X.; Gabayno, J.L.; Chen, H.T. Design and implementation of shape memory alloy-actuated nanotweezers for nanoassembly. *J. Micromech. Microeng.* **2014**, *24*, 095012.
102. Villanueve, A.; Smith, C.; Priya, S. A biomimetic robotic jellyfish (Robojelly) actuated by shape memory alloy composite actuators. *Bioinspir. Biomim.* **2011**, *6*, 036004.
103. Clausi, D.; Gradin, H.; Braun, S.; Peirs, J.; Stemme, G.; Reynaerts, D.; van der Wijngaart, W. Robust actuation of silicon MEMS using SMA wires integrated at wafer-level by nickel electroplating. *Sens. Actuators A Phys.* **2013**, *189*, 108–116.
104. Gabriel, K.J.; Trimmer, W.S.N.; Walker, J.A. A micro rotary actuator using shape memory alloys. *Sens. Actuators* **1988**, *15*, 95–102.
105. Mineta, T.; Deguchi, T.; Makino, E.; Kawashima, T.; Shibata, T. Fabrication of cylindrical micro actuator by etching of TiNiCu shape memory alloy tube. *Sens. Actuators A Phys.* **2011**, *165*, 392–398.
106. Mineta, T.; Kudoh, S.; Makino, E.; Kawashima, T.; Shibata, T. Accurate and simple assembly process of shape memory alloy tubular micro manipulator with a bias mechanism. *Microelectron. Eng.* **2011**, *88*, 2683–2686.
107. Chan, K.C.; Godman, M.J.; Walsh, K.; Wilson, N.; Redington, A.; Gibbs, J.L. Transcatheter closure of atrial septal defect and interatrial communications with a new self expanding nitinol double disc device (Amplatzer septal occluder): Multicentre UK experience. *Heart* **1999**, *82*, 300–306.
108. Kaufman, J.A.; Geller, S.C.; Brewster, D.C.; Fan, C.-M.; Cambria, R.P.; Lamuraglia, G.M.; Gertler, J.P.; Abbott, W.M.; Waltman, A.C. Endovascular repair of abdominal aortic aneurysms: Current status and future directions. *Am. J. Roentgenol.* **2000**, *175*, 289–302.
109. Uflacker, R.; Robison, J. Endovascular treatment of abdominal aortic aneurysms: A review. *Eur. Radiol.* **2001**, *11*, 739–753.
110. Pass, R.H.; Hijazi, Z.; Hsu, D.T.; Lewis, V.; Hellenbrand, W.E. Multicenter USA amplatzer patent ductus arteriosus occlusion device trial: Initial and one-year results. *J. Am. Coll. Cardiol.* **2004**, *44*, 513–519.
111. Barras, C.D.J.; Myers, K.A. Nitinol—Its use in vascular surgery and other applications. *EJVES Extra* **2010**, *19*, 564–569.
112. Torrisi, L. The NiTi superelastic alloy application to the dentistry field. *Biomed. Mater. Eng.* **1999**, *9*, 39–47.
113. Sattapan, B.; Palamara, J.E.; Messer, H.H. Torque during canal instrumentation using rotary nickel-titanium files. *J. Endod.* **2000**, *26*, 156–160.
114. Laster, Z.; MacBean, A.D.; Ayliffe, P.R.; Newlands, L.C. Fixation of a frontozygomatic fracture with a shape-memory staple. *Br. J. Oral Maxillofac. Surg.* **2001**, *39*, 324–325.
115. Wang, Y.; Zheng, G.; Zhang, X.; Zhang, Y.; Xiao, S.; Wang, Z. Temporary use of shape memory spinal rod in the treatment of scoliosis. *Eur. Spine J.* **2011**, *20*, 118–122.
116. Lekston, Z.; Stroz, D.; Drusik-Pawlowska, M.J. Preparation and characterization of nitinol bone staples for cranio-maxillofacial surgery. *J. Mater. Eng. Perform.* **2012**, *21*, 2650–2656.

117. Levi, D.S.; Kusnezov, N.; Carman, G.P. Smart materials applications for pediatric cardiovascular devices. *Pediatr. Res.* **2008**, *63*, 552–558.
118. Di Mitri, R.; Mocciaro, F. The new nitinol conformable self-expandable metal stents for malignant colonic obstruction: A pilot experience as bridge to surgery treatment. *Sci. World J.* **2014**, *2014*, 651765.
119. Rajan, G.P.; Eikelboom, R.H.; Anandacoomaraswamy, K.S.; Atlas, M.D. *In vivo* performance of the nitinol shape-memory stapes prosthesis during hearing restoration surgery in otosclerosis: A first report. *J. Biomed. Mater. Res. Part B Appl. Biomater.* **2005**, *72*, 305–309.
120. Avgoustou, C.; Penlidis, P.; Tsakpini, A.; Sioros, C.; Giannousis, D. Compression anastomoses in colon and rectal surgery with the NiTi ColonRing™. *Tech. Coloproctol.* **2012**, *16*, 29–35.
121. Lee, A.P.; Ciarlo, D.R.; Krulevitch, P.A.; Lehew, S.; Trevino, J.; Northrup, M.A. A practical microgripper by fine alignment, eutectic bonding and SMA actuation. *Sens. Actuators A Phys.* **1996**, *54*, 755–759.
122. Huang, W.M.; Tan, J.P.; Gao, X.Y.; Yeo, J.H. Design, testing, and simulation of NiTi shape-memory-alloy thin-film-based microgrippers. *J. Microlithogr. Microfabr. Microsyst.* **2003**, *2*, 185–190.
123. Lan, C.-C.; Lin, C.-M.; Fan, C.-H. A self-sensing microgripper module with wide handling ranges. *IEEE/ASME Trans. Mechatron.* **2011**, *16*, 141–150.
124. Houston, K.; Eder, C.; Sieber, A.; Menciassi, A.; Carrozza, M.C.; Dario, P. Polymer sensorised microgrippers using SMA actuation. In Proceedings of the 2007 IEEE International Conference onRobotics and Automation, Roma, Italy, 10–14 April 2007; pp. 820–825.
125. Zhang, H.J.; Qiu, C.J. A TiNiCu thin film micropump made by magnetron Co-sputtered method. *Mater. Trans.* **2006**, *47*, 532–535.
126. Hsu, Y.-C.; Lin, S.-J.; Hou, C.-C. Development of peristaltic antithrombogenic micropumps for *in vitro* and *ex vivo* blood transportation tests. *Microsyst. Technol.* **2008**, *14*, 31–41.
127. Graf, N.J.; Bowser, M.T. A soft-polymer piezoelectric bimorph cantilever-actuated peristaltic micropump. *Lab Chip* **2008**, *8*, 1664–1670.
128. Guo, S.; Sun, X.; Ishii, K.; Guo, J. SMA actuator-based novel type of peristaltic micropump. In Proceedings of the 2008 IEEE International Conference on Information and Automation, (ICIA 2008), Changsha, China, 20–23 June 2008; pp. 1620–1625.
129. Shkolnikov, V.; Ramunas, J.; Santiago, J.G. A self-priming, roller-free, miniature, peristaltic pump operable with a single, reciprocating actuator. *Sens. Actuators A Phys.* **2010**, *160*, 141–146.
130. Guo, S.; Fukuda, T. SMA actuator-based novel type of micropump for biomedical application. In Proceedings of the IEEE International Conference on Robotics and Automation, New Orleans, LA, USA, 26 April–1 May 2004; pp. 1616–1621.
131. Xia, L.; Wang, F.; Lu, J. A valveless micropump driven by differential SMA actuator. *Proc. SPIE* **2007**, *6423*, doi:10.1117/12.779366.